Applied Physics B (2023) 129:97
https://doi.org/10.1007/s00340-023-08038-3

Applied Physics B
Lasers and Optics

RESEARCH

Characterization of laser-induced emission of high-purity TiO_2 nanoparticles: feasibility of laser-induced incandescence

Junghwa Yi[1] · Christopher Betrancourt[1] · Nasser Darabiha[1] · Benedetta Franzelli[1]

Received: 14 January 2023 / Accepted: 4 May 2023 / Published online: 23 May 2023

Abstract
The development of laser-induced incandescence (LII) approach for characterizing the production of high-purity non-carbonaceous metal oxides produced in flame synthesis systems is in progress. This work aims to prove the feasibility of LII measurement for titanium dioxide (TiO_2). In previous works, laser-induced emission (LIE) was investigated for flame-synthetized TiO_2 particles. However, the presence of carbon materials was detected. As this calls into question the nature of the signal, we consider in this work LIE of high-purity engineered TiO_2 nanoparticles to circumvent the carbon issue. Specifically, we investigate the spectral and temporal laser-induced emissions of pure TiO_2 nanoparticles dispersed in a non-reactive environment. In parallel, LIE from carbon black is examined to validate the strategy and highlight differences between carbon black and TiO_2. The TiO_2 results indicate that depending on the laser fluence, different prompt interferences appear. The literature suggests that these non-thermal emissions are likely to be from fluorescence or phase-selective laser-induced breakdown spectroscopy, both characterized by a short lifetime. To avoid these parasitic signals, measurement acquisition time is delayed. A spectral red-shift is observed with time as a result of decreasing particle temperature. This proves the LII nature of delayed emission from pure TiO_2, which is confirmed by the LII-like nature of the temporal signals.

1 Introduction

Titanium dioxide (TiO_2, titania) nanomaterials are the second most produced powders through flame synthesis technology [1] following carbon black. They are widely used for pigment, cosmetics, and semiconductors [2]. With its unique photocatalytic properties, TiO_2 also gets more attention in wastewater treatment [3] and solar power systems [4].

Flame synthesis technology can control the final product characteristics with a wide versatility through the choice of reactants and precursors, mixture composition, residence time, and temperature experienced by the particles [5]. These operating conditions are closely related to the history of the particles, i.e., the local gaseous conditions experienced by the particles along their trajectory that play an important role on the physicochemical properties of the final product: shape, size, surface functionality, crystallinity, and particle coating [6–8]. As an example, Cignoli et al. [9] showed via X-ray diffraction (XRD) that TiO_2 crystal phase changes from anatase to rutile along the height of a premixed lean methane–air flame doped with TTIP (titanium tetraisopropoxide, $Ti(OC_3H_7)_4$) precursor.

Therefore, there is a crucial need to understand the detailed physical and chemical processes involved in non-carbonaceous nanoparticles formation in flames to control the final product characteristics. Specifically, experimental databases with accurate measurements of volume fraction (f_v), size distribution, and local flame conditions in steady laminar flames are demanded to understand and characterize the particle formation processes: inception, growth, agglomeration, and phase changing of TiO_2 nanoparticles along the

✉ Christopher Betrancourt
christopher.betrancourt@centralesupelec.fr

✉ Benedetta Franzelli
benedetta.franzelli@centralesupelec.fr

Junghwa Yi
junghwa.yi@centralesupelec.fr

Nasser Darabiha
nasser.darabiha@centralesupelec.fr

[1] Laboratoire EM2C, Université Paris-Saclay, CNRS, CentraleSupélec, Gif-sur-Yvette 91190, France

flame. Such databases are also required to develop and evaluate the performances of CFD models for non-carbonaceous nanoparticles production in flame synthesis.

Classically, ex situ and online diagnostics are used for characterizing the produced particles. For example, transmission electron microscopy (TEM) [10] provides primary particle size and morphology of sampling, and an online scanning mobility particle sizer (SMPS) can be used to measure the mobility diameter. The particle size obtained with ex situ or online methods may differ from those found in actual flame conditions, since the sampling method including extraction, deposition and/or filtration may lead to losses and coagulation [11, 12].

Alternatively, in situ optical techniques can be used for describing the evolution of the particle properties along the flame because of their absent or weak intrusive nature. In this sense, laser diagnostics techniques are well adapted to this purpose. Several laser techniques have been used to characterize various nanoparticle properties based on the laser-induced emission of TiO_2. Three techniques are mainly considered in the literature for solid phase description: laser-induced fluorescence (LIF), phase-selective laser-induced breakdown spectroscopy (PS-LIBS), and laser-induced incandescence (LII).

Laser-induced fluorescence, often referred to as photoluminescence (PL), generally uses a laser of few mW (in case of commercial spectrophotometer) to excite electrons to an excited state and relax to the ground state through various processes with a typical lifetime from ps to tens of ns [13]. TiO_2 LIF spectra excited by using UV laser presents a wide range of band emissions [14], since it strongly depends not only on particle intrinsic properties (size [15], morphology [16], crystal state [17], and chemical or thermal surface treatment [18]), but also on LIF operation conditions (excitation laser wavelength [19], chemical environment [19], and temperature [20, 21]). For example, even for an identical TiO_2 atomic structure, the LIF spectra show different shapes in the visible range due to different surface geometry and relaxation processes of photo-generated carriers at the surface [19]. To obtain in situ measurements, the LIF emission should be quantitatively measured along the flame. Nevertheless, due to its complex nature and strong dependence on environment and particle characteristics, the interpretation of the signal is challenging without a prior and robust description of TiO_2 LIF emission mechanisms.

Phase-selective laser-induced breakdown spectroscopy (PS-LIBS) uses laser fluence in between the breakdown thresholds of gas and particle phases. Using PS-LIBS, information can be obtained on gas-to-particle conversion [22], volume fraction measurement [23, 24], and band gap variation in mixed crystal structures [25]. Therefore, PS-LIBS could be a promising in situ technique to investigate TiO_2 formation in flame. However, its application requires a relatively high laser fluence level from ~ 1 to 60 J/cm^2 [26–28], typically at 355 nm and 532 nm, which may make PS-LIBS intrusive.

Laser-induced incandescence uses a pulsed laser to heat the particles. The particles absorb the laser radiation and reach a high temperature. The heated particles emit thermal radiation, i.e., incandescent signal, during their cooling by conduction, convection, and vaporization. The incandescent signal contains information on volume fraction and primary particle size [29, 30]. This technique, initially developed for measuring the volume fraction and size of soot particles in flames [31], has attracted attention in the application to non-soot nanoparticle flame synthesis such as various metals (Fe [32], Si [33], Mo [34]), oxides (SiO_2[35], Al_2O_3 [36], Fe_2O_3 [37]), and complex carbon-coated materials [8, 38, 39].

Regarding TiO_2 nanoparticles, pioneering works on flame-synthesized particles can be found in literature [8, 9, 40–42]. However, when TiO_2 nanoparticles are produced via flame synthesis, the carbon content of the precursors and of the fuel used in the pilot flame may lead to the generation of soot [43] or carbon-coated TiO_2 nanoparticles [8, 43]. This solid carbon content can significantly change the LII signal with distinct optical properties [44]. Thus, to our knowledge, the feasibility of the LII technique for high-purity TiO_2 nanoparticles, i.e., without carbon presence, has not been deeply explored.

In this framework, the scope of this work is to characterize the laser-induced emission of high-purity TiO_2 nanoparticles to demonstrate the feasibility of the LII technique when considering TiO_2 without carbon content.

The main challenge for the application of LII on flame synthesis TiO_2 (but also other flame-synthesized particles) compared to carbonaceous nanoparticles is related to the specific optical properties of TiO_2. Performing LII on TiO_2 supposes that the particles absorb laser radiation. The absorption function $E(m_\lambda)$ translates this ability [45]. $E(m_\lambda)$ is a function of the refractive index (m) at a wavelength (λ). Figure 1 displays the absorption function $E(m_\lambda)$ of carbonaceous particles (e.g., soot) [46–49] and TiO_2 from various sources of literature [50–54]. It should be noticed that $E(m_\lambda)$ values for TiO_2 are illustrated using a log-scale. The $E(m_\lambda)$ of TiO_2 as a function of wavelength exhibits inconsistencies across various studies. All measurements are remarkably small, a few orders of magnitude smaller than carbonaceous particles. TiO_2 has a better absorption in the UV part, which decreases significantly on the visible range except for De Iuliis et al. [54] with a nearly constant $E(m_\lambda)$ in the UV–visible range.

The $E(m_\lambda)$ tendency of TiO_2 highlights two main issues. First, it is recommended to heat TiO_2 particles using a UV laser to improve heat-up efficiency [12], which is not

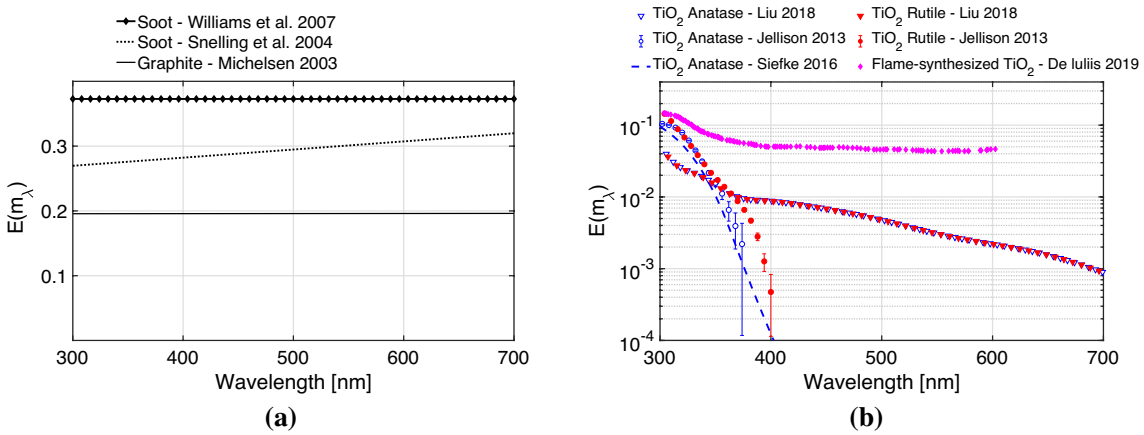

Fig. 1 Absorption function $E(m_\lambda)$ of **a** carbonaceous particle [46, 49, 55] and **b** TiO_2 nanoparticles (in log-scale) [51–54]

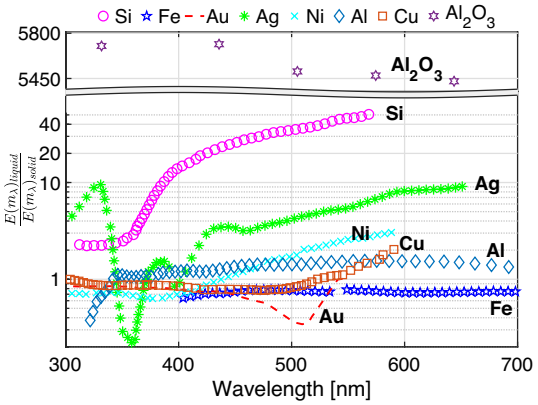

Fig. 2 Ratio of liquid and solid phase $E(m_\lambda)$. Si and Fe from [12]; solid Au, Ag, and Ni from [12] and liquid Au, Ag and Ni from [59]; Al, Cu from [59]; Al_2O_3 from [60]

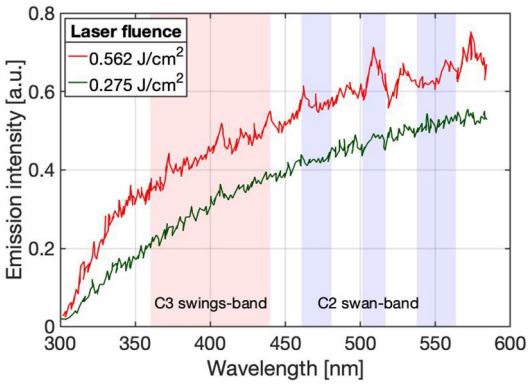

Fig. 3 Laser-induced light emission under different laser fluences at HAB = 2 cm in flame spray synthesis of TiO_2 nanoparticles at prompt detection timing obtained in [42]. C_2 and C_3 bands from [61] are indicated in blue and red, respectively

recommended in flame since it may lead to interferences due to gaseous species fluorescence in LII measurement [56]. Second, since $E(m_\lambda)$ values for TiO_2 are quite small compared to those of soot, the potential laser incandescence signal emitted in the visible range for an equivalent volume fraction of TiO_2 particles will be weaker by few orders of magnitude than soot particles.

De Iuliis et al. [42] conducted LII on in situ flame-synthesized TiO_2 using a 1064 nm laser despite the quasi-null absorption function at this wavelength [57]. Two hypotheses might explain the detection of the LII signal on TiO_2 under IR excitation. First, the reported flame temperatures via pyrometry (2800–3000 K [42, 54]) are much higher than the typical TiO_2 melting point (about 2100 K [58]). Therefore, the nanoparticles in the flame could be in a liquid state so that they could absorb the IR laser radiation. In such a case, the physical properties for interpretation of the LII signal should be well adjusted in liquid phase materials. To illustrate this, Fig. 2 shows the ratio of liquid and solid phase $E(m_\lambda)$ as a function of the wavelength for several metal particles and Al_2O_3. Ni, Au, Cu, Al, and Fe have spectrally different absorption functions when they are in a liquid state, fluctuating close to 1. Ag, Si, and Al_2O_3 have a much higher absorption function in a liquid state.

Thus, the in situ LII under IR excitation on flame-generated TiO_2 nanoparticles in [42] might be explained if they were in a liquid state, which may substantially increase their absorption function. Unfortunately, to the author's knowledge, information on the optical property of molten TiO_2 is not available in the literature to confirm this hypothesis.

The second hypothesis is that these flame-generated nanoparticles are not pure TiO_2 nanoparticles. The prompt LII spectra obtained from TiO_2 nanoparticle flame spray synthesis using a 1064 nm laser in [42] at moderate (F = 0.275 J/cm^2) and high (F = 0.562 J/cm^2) fluences are recalled in Fig. 3. Induced bands' emission of C_2 swan and

C_3 swings [61] can be recognized. The swan and swing band emissions at high fluence are characteristic of solid carbon contents in the form of soot particles or carbon-coated TiO_2. Specifically, Ren et al. [8] showed using PS-LIBS that an increase in C_2 emission indicates an increase of carbon components in the produced carbon-coated TiO_2 nanoparticles.

The above short review of the LII technique application on flame-synthesized TiO_2 nanoparticles highlights the importance of working with high-purity TiO_2 nanoparticles. Additionally, when performing ex situ LII measurements using UV radiation on flame-synthesized TiO_2 nanoparticles, De Iuliis et al. [54] showed that the nature of the laser-induced emission (LIE) has to be carefully analyzed, since parasitic signals were observed in the prompt emission spectra in both low and high fluence regimes. These additional signals were not extensively characterized without the matrix effect of sampling filter [54].

An extensive characterization of the LIE at prompt and delayed acquisition of high-purity TiO_2 nanoparticles in a well-controlled environment is the core of the present study. For this, an aerosol made of commercial high-purity TiO_2 nanoparticles produced via sol–gel process is transported by a nitrogen flow in an optical cell at room temperature. This permits avoiding the risk of (1) melting caused by the local environment, ensuring a solid state prior to laser interaction, (2) interferences from carbon-related species during the measurements, and (3) parasitic signal from gaseous species characterizing flame environment. The effect of laser fluence and delay time with respect to the signal peak is investigated and compared to well-known carbon black nanoparticle LIE acquired in the same condition. For different laser excitation and signal detection schemes, various explanations are explored to interpret the LIE of TiO_2 nanoparticles by combining information from spectra and temporal evolution of the signals. The feasibility of LII on pure TiO_2 aerosol in a cold environment is then demonstrated. This study is organized as follows. First, the scientific strategy to investigate the nature of LIE is presented in Sect. 2. Then, the experimental setup is described in Sect. 3. Finally, the experimental results are discussed in Sect. 4. To complete this study, the same strategy has also been applied to flame-synthesized TiO_2 in a coflow H_2/AR flame. These results are reported in the Supplementary material.

2 Scientific strategy to analyze LIE

Three different types of laser-induced emissions (LIEs) from TiO_2 nanoparticles are considered here: laser-induced fluorescence, phase-selective laser-induced breakdown spectroscopy, and laser-induced incandescence.

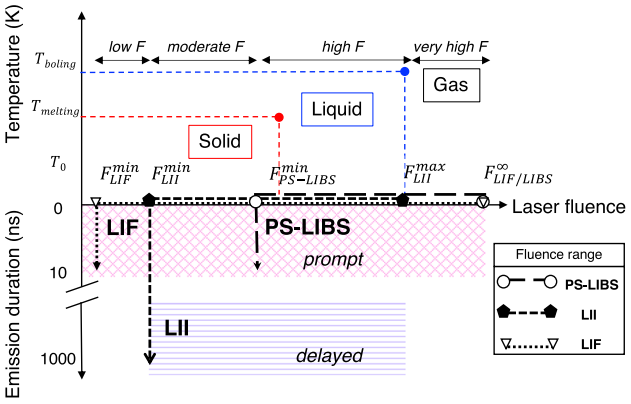

Fig. 4 Schematic presentation of the particle phase information related to the temperature (top) and to the LIE characteristic emission duration (bottom) as a function of the typical fluence range of different LIE signals

In conventional LIBS, the plasma mainly emits a continuous spectrum from Bremsstrahlung emission and the recombination radiation at the tens to hundreds of nanoseconds. Upon cooling of the plasma, the relative peak intensity of ion/atom line emissions increases significantly. The behavior of the plasma and the quantitative nature of the emitted temporal evolution can substantially vary (up to ms) depending on the materials and experimental conditions, including the gas temperature and excitation wavelengths. On the other hand, the lifetime of PS-LIBS is reported to be shorter (a few tens of nanoseconds) than those of conventional LIBS due to the absence of gaseous plasma (See Table 1). In this study, no conventional LIBS is expected to occur, since the fluence regime used in this work is always lower than the air breakdown threshold (~ 100 J/cm^2 at 355 nm [62]). As a confirmation, no visible spark was observed.

The three considered LIEs can simultaneously occur during the laser excitation as illustrated in Fig. 4, which displays the schematic of the fluence range of LIE with their corresponding emission duration and the corresponding particle phase (solid, liquid, and gas). The various LIEs of TiO_2 nanoparticles have different characteristic times and occur under different fluence regimes as summarized in Table 1. Thus, by examining the time and laser fluence dependence of the spectral emissions from TiO_2, the nature of the detected signal can be characterized.

First, the general spectral characteristics of LII will be presented in Sect. 4.1 to clarify the retained strategy. Then, prompt LIE will be deeply investigated in Sect. 4.1.1. Specifically, TiO_2 LIF is expected to be the only emission observed at low laser fluence regimes, where neither LII nor PS-LIBS is expected, as indicated in Fig. 4. Then, by increasing the laser fluence, the TiO_2 particle temperature is expected to rise, and different spectral features of TiO_2 fluorescence could be induced [20]. From moderate to high laser fluence

Table 1 Characteristics of the laser-induced emissions of TiO_2 nanoparticles in terms of operating fluence range and characteristics time (at 1 atm)

Laser λ_{ex}	LIF	PS-LIBS	LIBS	LII
UV	Continuous wave (~ mW)	0.4–32 J/cm^2 at 355 nm [63]	–	0.0007-–0.05 J/cm^2 (filter) 0.08-–0.15 J/cm^2 (flame) at 266 nm [54]
532 nm	–	1.6–56 J/cm^2 [25, 63, 64]	–	–
1064 nm	–	10–45 J/cm^2 [64]	24–75 J/cm^2 [65, 66]	0.01-–0.56 J/cm^2 [42]
Characteristic time	ps to 10 ns [13]	10 ns [27]	300 ns–ms [67]	10^2–10^3 ns

regimes, the LIF, PS-LIBS, and LII of the TiO_2 nanoparticles could occur simultaneously with different intensities which makes analyzing the signal very challenging. Finally, a delay on the signal detection is introduced in Sect. 4.1.2, so that LIF and PS-LIBS emission signals, classically lasting for the excitation laser duration (FWHM 5 ns in this study), are not expected to be found. Thus, under different laser fluence regimes, the time-resolved behavior of delayed TiO_2 emission spectra is investigated using LII theory to demonstrate its LII nature. These aspects will be reviewed using a temporal description in Sect. 4.2. All TiO_2 measurements are compared with those of carbon black particles as a representative LII behavior under laser irradiation.

2.1 LII theory

The evolution of the LII signal emitted at wavelength λ_{em} by a heated spherical particle with diameter d_p at temperature $T_p(t)$ during its cooling is expressed by:

$$S_{LII}(\lambda_{em}, d_p(t)) = \frac{4\pi^2 d_p^3 E(m_{\lambda_{em}})}{\lambda_{em}} \frac{2h\pi c^2}{\lambda_{em}^5} \left[\exp\left(\frac{hc}{\lambda_{em} k_B T_p(t)}\right) - 1\right]^{-1}, \quad (1)$$

with $E(m_{\lambda_{em}})$ the absorption function of particle at λ_{em}, h the Planck's constant, c the light speed, and k_B the Boltzmann's constant. To confirm the LII nature of LIE, theoretical evolution of the signal is examined using the following three points:

- The spectral emission as a function of temperature has to be verified. The peak location of the spectrum is expected to move toward longer wavelengths (red-shifted) with decreasing temperature or toward shorter wavelengths (blue-shifted) with increasing temperature, i.e., the spectrum has to follow Wien's displacement law. This thermal shift is valid only if $E(m_{\lambda_{em}})$ is invariant with particle temperature. Therefore, if the particles undergo a physical phase change from liquid to solid during their cooling, this assertion becomes questionable since the particle phase change may include a variation of the absorption function as illustrated in Fig. 2. The spectral analysis will be presented in Sect. 4.1.
- The temporal decay characteristic time under different detection wavelengths will be employed to distinguish temporally incandescence signals from other emissions in Sect. 4.2. More precisely, LII signal $S_{LII}(\lambda_{em}, T_p(t))$ is a function of emission wavelength λ_{em} (Eq. 1). If $d_p(t)$ and $E(m_{\lambda_{em}})$ are assumed to be constant[1] during the LII decay, by putting a natural log on both sides of Eq. (1), it can be obtained that:

$$\ln(S_{LII}(\lambda_{em}, T_p(t))) = \ln C - \ln\left(\exp\left(\frac{hc}{\lambda_{em} k_B T_p(t)}\right) - 1\right), \quad (2)$$

with $C = 8\pi^3 d_p^3 h c^2 E(m_{\lambda_{em}}) \lambda_{em}^{-6}$. Considering C to be constant during the time range $[t_i, t_j]$, a decay characteristic time τ can then be defined as:

$$\tau = \frac{t_i - t_j}{\ln(S_{LII}(t_i)) - \ln(S_{LII}(t_j))} = \frac{t_i - t_j}{\ln\left(\exp\left(\frac{hc}{\lambda_{em} k_B T_p(t_j)}\right) - 1\right) - \ln\left(\exp\left(\frac{hc}{\lambda_{em} k_B T_p(t_i)}\right) - 1\right)}. \quad (3)$$

Since $\frac{hc}{\lambda_{em} k_B T_p(t)} >> 1$, Wien's approximation can be applied:

$$\exp\left(\frac{hc}{\lambda_{em} k_B T_p(t_i)}\right) - 1 \approx \exp\left(\frac{hc}{\lambda_{em} k_B T_p(t_i)}\right),$$

so that:

$$\tau = \frac{k_B \lambda_{em}}{hc}(t_i - t_j)\left(\frac{1}{T_p(t_j)} - \frac{1}{T_p(t_i)}\right)^{-1}. \quad (4)$$

[1] Assuming $d_p(t)$ to be constant means that sublimation is negligible during the duration of the LII process.

It can be noted that the decay characteristic time τ is linearly proportional to the emission wavelength λ_{em}. This relationship is valid only for LII, meaning that if it is verified, interference signals like fluorescence or atomic emission are not present. It is worth mentioning that τ depends on the evolution of the particle temperature. Therefore, assuming that all particles attain the same temperature for a given fluence and a gas temperature, the decay characteristic time will be inversely proportional to the particle diameter.

- From Eq. (2), it is possible to derive that the quantity:

$$\Delta T^{-1}(t) = \frac{1}{T_p(t_0)} - \frac{1}{T_p(t)} = \ln\left[\frac{S_{\mathrm{LII}}(\lambda_{\mathrm{em}}, T_{\mathrm{p}}(t))}{S_{\mathrm{LII}}(\lambda_{\mathrm{em}}, T_{\mathrm{p}}(t_0))}\right] \left(\frac{hc}{\lambda_{\mathrm{em}} k_B}\right)^{-1} \tag{5}$$

is not dependent on the detection emission. Thus, if the measured emission is an LII signal, the following relation has to be verified:

$$\ln\left[\frac{S_{\mathrm{LII}}(\lambda_{\mathrm{em,i}}, T_{\mathrm{p}}(t))}{S_{\mathrm{LII}}(\lambda_{\mathrm{em,i}}, T_{\mathrm{p}}(t_0))}\right] \left(\frac{hc}{\lambda_{\mathrm{em,i}} k_B}\right)^{-1} = \ln\left[\frac{S_{\mathrm{LII}}(\lambda_{\mathrm{em,j}}, T_{\mathrm{p}}(t))}{S_{\mathrm{LII}}(\lambda_{\mathrm{em,j}}, T_{\mathrm{p}}(t_0))}\right] \left(\frac{hc}{\lambda_{\mathrm{em,j}} k_B}\right)^{-1}, \forall \lambda_{\mathrm{em,i}}, \lambda_{\mathrm{em,j}}. \tag{6}$$

In Sect. 4.2, the temporal estimation of $\Delta T^{-1}(t)$ will be calculated from PMT signals at two different λ_{em}. If identical, the LII nature of the signal at λ_{em} will be confirmed at least for the two considered wavelengths.

In the following, carbon black will serve as a reference case for typical LII behavior and compared to the TiO_2 LIE induced in similar operating conditions.

3 Experimental setup

The experimental setup considered in this work is constituted of three parts, as illustrated in Fig. 5: particle dispersion, laser setting, and signal detection.

3.1 Particle dispersion

A nanoparticle-laden aerosol is prepared with commercial particles of carbon black (nanografi, NG04EO0709, $d_p = 20$ nm, spherical) or TiO_2 (nanografi, Rutile (NG04SO3507), $d_p = 28$ nm, purity 99.995+%, produced by the sol–gel method). Nanoparticles are transported in a non-reactive environment thanks to N_2 flow (16.67 slm, 9.8 m/s) in a first flask (1 L) placed inside an ultrasonic water bath. The nanoparticle-laden gas stream passes through another buffer flask (1 L) to get a homogeneous distribution. Then, the

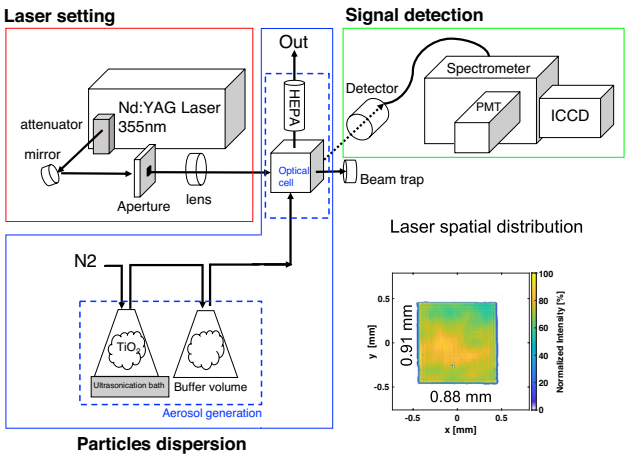

Fig. 5 Schematic presentation of the experimental setup developed to investigate laser-induced emission from TiO_2 nanoparticle-laden aerosol using a pulse YAG laser at 355 nm with a nearly top-hat spatial profile (bottom-right)

nanoparticles are dispersed in an optical cell, presenting two 1-inch opposite windows (UVFS, Thorlabs WG41010) for the laser path and a 2-inch window (UVFS, Thorlabs WG42012) for the detection system. Particles are evacuated by the top hood equipped with a HEPA filter.

Since the dispersion rate of the particles is decreasing over time, the particles inside the first flask are reloaded after each series of measurements with m_g= 200 mg of particles, allowing repeatable experimental conditions. This also means that only normalized signals will be considered in the following.

When changing the particle's nature (TiO_2 or carbon black), to prevent any intervention of particles from previous measurements, all the equipment components in contact with particles are entirely changed.

3.2 Laser setting

An Nd:YAG laser beam (Quantel, Q-smart 850) with a repetition rate of 10 Hz and pulse duration of 5 ns (FWHM) is used for the LII measurement. Operation wavelength was tested for three different harmonics—fundamental (1064 nm), second (532 nm), and third (355 nm)—on both carbon black and TiO_2 by adding harmonic generation modules to the laser head. The laser fluence is controlled using an attenuator consisting of a half-wave plate and two polarizers.

The beam presents a nearly top-hat energy distribution of 0.88×0.91 mm^2, which is monitored with a beam profiler (Gentec Beamage). It is represented in the bottom right in Fig. 5 and also as a histogram in Fig. 6. The nearly top-hat shape laser is then 1:1 relay imaged at the centerline of the optical cell.

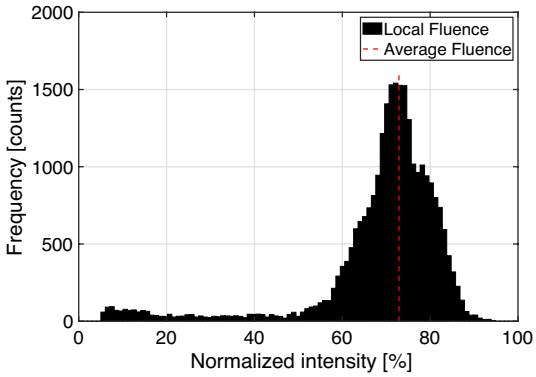

Fig. 6 Histogram of laser fluence across the laser beam detected by the beam profiler

3.3 Signal detection

The signal detection consists of a telescope comprising two achromatic lenses (f_1= 10 cm and f_2 = 20 cm). A magnification factor of 2 is used to collect the induced signal at 90° of the laser beam direction. Two notch filters (355 and 532 nm) were used to suppress the laser harmonic signal. For this reason, the emission spectra between 525 nm and 540 nm were excluded from all the results. This collector is connected to the spectrometer entrance (Princeton Instruments, HRS-500, grating groove density of 150 groove/mm) through a multimode optical fiber (Thorlabs, FG365UEC) with a core diameter of 365 µm. The probe volume is 0.58 mm^3. One exit of the spectrometer is connected to an intensified charge-coupled device camera (ICCD, Princeton Instruments, PI-MAX 4 1024EMB) to measure the spectral emission of LII with a gate width of 20 ns. The temporal behavior of laser-induced emission spectra is measured by considering different acquisition gate delay times (τ_d = 0–500 ns with respect to the signal peak). The detection system is calibrated using a tungsten filament lamp for signal intensity and a mercury lamp for wavelength. The acquisition parameters are adapted to ensure the best signal-to-noise (S/N) ratio and to prevent saturation of the device. The intensity level is then rescaled to be treated on the same intensity scale. The spectra displayed in this work are averaged over 5000 single shots.

The time-resolved laser-induced emission was measured using a visible photomultiplier (PMT, HAMAMATSU, R2257), which is connected to the second exit slit of the spectrometer. Signals at four different wavelengths (λ_{em} = 450, 570, 640, and 710 nm for carbon black, and λ_{em} = 450, 550, 650, and 710 nm for TiO_2) with detection bandwidth of FHWM 20 nm were measured. The choice of detection wavelengths was considered to cover the visible range of the spectrum to represent the temporal evolution of LIE signals for overall wavelengths. However, to avoid interferences at the prompt stage as much as possible and to capture the LII behavior, the choice of wavelengths between carbon black and TiO_2 was slightly different (570 nm and 640 nm for carbon black; 550 nm and 650 nm for TiO_2). The acquired PMT signals were recorded at 10 Hz using an oscilloscope (Lecroy wave surfer 434, 350 MHz bandwidth, 2 GS/s sampling rate). As the particle dispersion rate decreases, the signal intensity also decreases, and so does the S/N ratio. To overcome this issue, only the PMT signals with the same order of S/N are kept, then normalized by their maximum intensity, and averaged over 6000 single shots.

Table 2 Detectable LIE signals with our detection system for different laser wavelengths for carbon black and pure TiO_2 nanoparticles

Wavelengths	1064 nm	532 nm	355 nm
Carbon black	YES	YES	YES
TiO_2	NO	NO	YES

Even though the absolute intensity would provide significant additional insight, due to the nature of the particle dispersion system, the measurement of absolute intensity cannot be guaranteed in the current system, since the amount of materials in the optical cell decreases with time. This means that during the acquisition performed over 2–3 min, the emission level decreases. Nevertheless, it has been verified that the normalized spectral and temporal behavior yielded the same stable results. Therefore, all the data are presented in a normalized form by their own maximum or values at specific wavelengths that will be provided in the following.

4 Results and discussion

The first step of this work consisted of testing three laser wavelengths (1064 nm, 532 nm, and 355 nm) to induce LIE of pure TiO_2 and to compare the results to those obtained for carbon black in similar conditions (Table 2). For carbon black, laser-induced emission was detected for all excitation wavelengths. On the contrary, for pure TiO_2 it was not possible to detect a signal with the considered detection system when working at 532 nm and 1064 nm. This is likely to be due to the fact that the absorption function $E(m_{\lambda_{em}})$ of pure TiO_2 above the UV range is much lower than that of carbonaceous particles as shown in Fig. 1. Therefore, only the 355 nm laser wavelength is used in the following to study the LIE of pure TiO_2 and carbon black particles.

First, LIE is characterized with a spectral analysis in Sect. 4.1. Prompt and delayed spectra are detailed in Sects. 4.1.1 and 4.1.2, respectively. In Sect. 4.2, the temporal evolution of the LIE signals obtained using PMT is analyzed to confirm and complete the conclusions drawn from the spectral analyses.

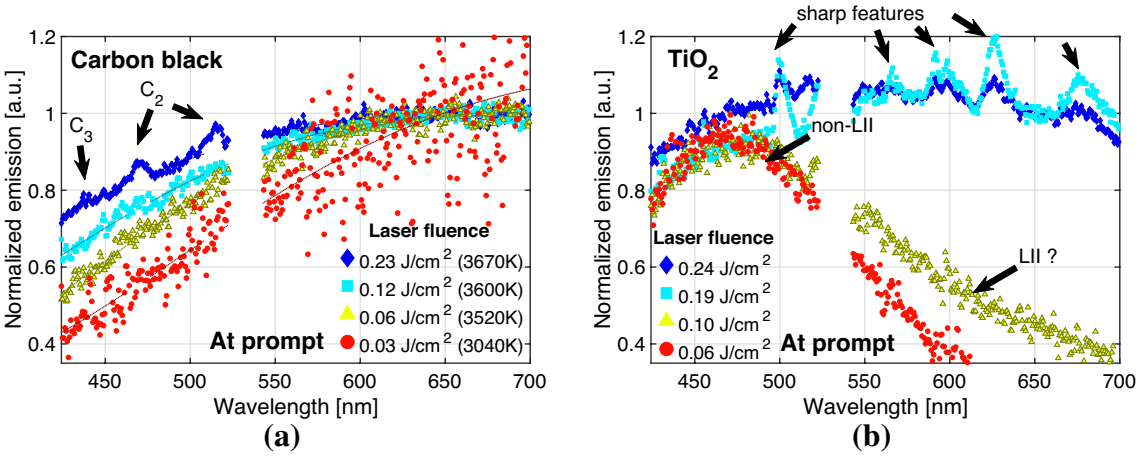

Fig. 7 Effect of laser fluence F on laser-induced emission spectra at prompt time for **a** carbon black and **b** TiO_2 nanoparticles. The temperature inside the legend for carbon black particles is obtained from the spectrum fitting of the Planck function. Spectra are normalized by the value at 650 nm, except for the case of TiO_2 $F = 0.06$ J/cm^2 and $F = 0.10$ J/cm^2, which are normalized by max value at 470 nm for visualization purpose

4.1 Spectral analysis

Fig. 7 shows the spectra under different laser fluences in prompt measurements. The equivalent temperature T_{eq} is obtained for carbon black by fitting the spectrum into Planck's law (Eq. 1) while considering $E(m_{\lambda_{em}})$ constant. The obtained T_{eq} value is reported in the legend of Fig. 7a.

A large variation of the spectral form of absorption function in the visible range has been discussed in Fig. 1 for TiO_2. Based on this, it would be unreliable to apply the fitting to extract the temperature information for TiO_2 from spectra of Fig. 7b.

Concerning carbon black, a laser fluence of $F = 0.03$ J/cm^2 is the minimum fluence to obtain an LII signal with a high enough S/N to be detected with our detection system. Still, the S/N is not high enough to allow accurate signal characterization. The case of $F = 0.03$ J/cm^2 will then not be considered further in the following. For all the considered fluences, the LIE signals exhibit continuous spectra in the visible wavelength range with low intensity for the shortest wavelengths. When increasing the laser fluence, the curve moves toward shorter wavelengths. This blue shift indicates that particle temperatures increased, as confirmed by the T_{eq} value. This trend follows Wien's displacement law, confirming the expected LII nature of the LIE signals for carbon black particles. By looking at the values of T_{eq}, it is found that the temperature increases with fluence for F < 0.12 J/cm^2, whereas it does not considerably change between 0.12 and 0.23 J/cm^2 while approaching the particle sublimation temperature.

Additionally, for the highest fluence ($F = 0.23$ J/cm^2), C_2 LIF signals (at approximately 468 nm and 516 nm) and some C_3 bands (at approximately 437 nm) are clearly noticed. This indicates the presence of sublimation of soot particles. All these results are coherent with the literature [68–70]. Especially when considering LII of soot particles produced in a premixed methane/air flame with a 355 nm laser, a laser fluence level of approximately 0.07 J/cm^2 is enough to reach the "plateau" region, i.e., the maximum temperature that soot particles attain when subjected to laser excitation [68]. In the present case, it might be possible that sublimation occurs for fluence values as small as F = 0.06 J/cm^2, but its effect on particle diameter is expected to be negligible since neither C_2 nor C_3 bands are observed.

The prompt emission spectra of pure TiO_2 particles show, on the contrary, a clearly different tendency as a function of laser fluence. At low fluence ($F = 0.06$ J/cm^2), a relatively narrow continuous spectrum centered at 470 nm is observed. This signal does not seem to correspond to LII emission that is expected to cover the whole visible range. For $F = 0.1$ J/cm^2, the spectrum covers a wider region, reaching the longest wavelengths (550–700 nm). As the laser fluence additionally increases ($F = 0.19$ and 0.24 J/cm^2), the emissions present a broadband continuous spectrum in the visible range with some sharp features. Compared to the broadband emission, these peaks are less significant at $F = 0.24$ J/cm^2 than at F = 0.19 J/cm^2. This possibly indicates that the relative contribution of the broadband spectrum to the total emission is likely to increase with laser fluence. As the interpretation of the prompt LIE of pure TiO_2 particles is not straightforward, a deep characterization in terms of LIF, PS-LIBS, and LII emissions is detailed in the next section.

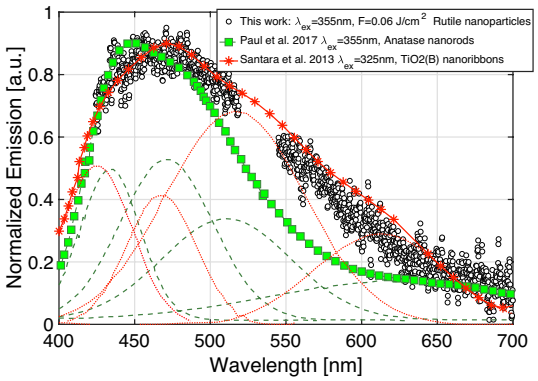

Fig. 8 Emission spectra of TiO_2 nanoparticles at prompt detection timing under laser fluence $F = 0.06$ J/cm^2 (black round points). The LIF emission spectra (square and star symbol) are from Gaussian fitted spectra (green dashed line from Paul et al. [72], red dotted lines from Santara et al. [73])

4.1.1 Characterization of prompt LIE from TiO_2

In the previous section, it has been observed that the behavior of prompt spectra emitted by carbon black is in agreement with the literature trends [71]. On the contrary, LIE from high-purity TiO_2 still needs to be characterized. In this section, the nature of the prompt LIE from TiO_2 is discussed as a function of the laser fluence.

As seen previously, in the low laser fluence regime, TiO_2 nanoparticles present a narrow emission centered at 470 nm. At low fluence, PS-LIBS is not expected, and LII is usually a signal covering the whole visible spectrum. Therefore, the emission observed at low laser fluences is most likely to be LIF. To confirm such conclusion, the TiO_2 spectra emission for a low laser fluence ($F = 0.06$ J/cm^2) is shown in Fig. 8. The spectrum obtained here for TiO_2 rutile nanoparticles is quite similar to LIF emission spectra found in the literature even for different crystal phases [72, 73]. As an example, spectra in low laser fluence regimes from Paul et al. [72] for anatase nanorods and Santara et al. [73] for TiO_2(B) nanoribbons are added to Fig. 8 in green and in red, respectively. Each curve can be interpreted as the sum of the Gaussian fit sub-band emissions illustrated with thin dashed/dotted lines in Fig. 8. These observations allow us to assert that the prompt LIE of pure TiO_2 is dominated by its fluorescence in the low fluence laser regime excited at 355 nm.

When increasing the laser fluence ($F = 0.10$ J/cm^2), a wider spectrum (Fig. 7b) is emitted. A longer wavelength part appears in LIE spectrum for higher fluence $F = 0.1$ J/cm^2. This would be in contradiction with LIF behaviors as in [74] if the signal was only originated by LIF. This seems to indicate the presence of a second signal in addition to LIF, whose contribution to the total LIE is evident at long wavelengths where the LIF signal is less significant.

At higher fluences ($F \geq 0.19$ J/cm^2), the nature of multiple emissions can be investigated by looking at the prompt emission spectra of TiO_2 nanoparticles for $F = 0.19$ J/cm^2 in Fig. 9. A broadband emission in the visible range is observed together with the presence of pronounced peak emissions, whose origins are unknown. The nature of peak emissions is first analyzed. One might think it could correspond to the atomic emission from laser breakdown of TiO_2 (LIBS). However, the energy level is still lower than the typical LIBS [65]. Therefore, two possibilities can be considered to interpret these signals: LIF and/or PS-LIBS emissions.

To consider the first option, deconvoluted Gaussian band emissions from various literature works are illustrated

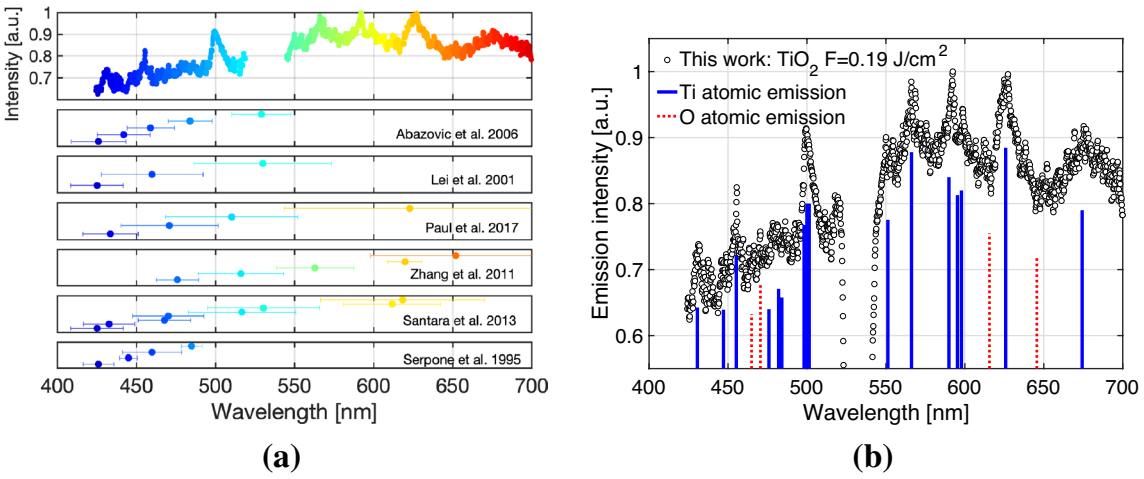

Fig. 9 Normalized emission spectra of TiO_2 for $F = 0.19$ J/cm^2 with **a** Gaussian fit of band emission of LIF from literature [15, 20, 72, 73, 75, 76] and **b** Ti and O atomic emissions from NIST [77] corresponding to peak location of emission spectra. The intensities of each transition are adapted for a clear view with the curve, not expressing the relative intensities

together with the emission spectra of TiO_2 in Fig. 9a. Only the center of each Gaussian band with the standard deviation $\pm\sigma$ range is shown for a clear view. The sub-bands from the literature cover almost all the distinct feature ranges of the spectrum. Therefore, the LIE can be the result of these different LIF contributions. As the laser fluence increases, it is possible for the positions of the sub-band peaks to remain unchanged while becoming progressively sharper, eventually achieving a line distribution [75]. This could be the first route to explain the edged features of the emission spectra of TiO_2 for high laser fluences.

Alternatively, it is possible to consider the distinct features as atomic emissions of PS-LIBS. Even though the laser fluence is relatively lower than the minimum PS-LIBS range in the literature (0.4 J/cm^2 at 355 nm in [63]), single-photon absorption may cause atomic emission following the mechanism proposed by [64] for PS-LIBS of flame-synthesized TiO_2. To consider this case, Ti and O atomic emissions from NIST are overlapped in blue and in red, respectively, to the emission spectrum of TiO_2 in Fig. 9b. The peak locations match fairly well with Ti and O atomic emissions.

The current results suggest that in a high laser fluence regime, prompt LIF and/or PS-LIBS of pure TiO_2 occurs. These emissions are expected to occur over a short period of time (Fig. 4). On the contrary, the broadband emission covers the whole visible spectrum, as expected for the LII signal. To confirm the LII nature of the broadband emission, laser-induced emissions at delayed acquisition time are investigated in the following section since LII is known to be a long-lasting signal.

4.1.2 LII nature of delayed LIE from TiO_2

As discussed previously, LIF and/or PS-LIBS signals of pure TiO_2 nanoparticles are observed at the prompt emission. Since LIF and PS-LIBS signals have a short characteristic decay time, it is possible to investigate the nature of the broadband contribution by looking at the delayed LIE of TiO_2. The trend as a function of gate delay and emission wavelength is here compared with the theoretical behavior for LII, which is described in Sect. 2.1 and with reference results from carbon black to prove its LII-like nature.

First, Fig. 10 shows the laser-induced emission spectra of carbon black and pure rutile TiO_2 particles at three fluence levels, at various acquisition delays (over 20 ns) from the prompt timing, i.e., the signal peak. For all laser fluences, the emission spectra of carbon black show a red shift when increasing the time delay. This indicates that the temperature decreases in agreement with LII theory as confirmed by the calculated equivalent temperatures reported in the legend.

Regarding TiO_2 nanoparticles, for the lowest fluence (F = 0.06 J/cm^2), the signal-to-noise ratio is not sufficiently high to obtain an exploitable spectrum for an acquisition delay as small as 20 ns. When looking at a higher laser fluence (F = 0.1 J/cm^2), a continuous broadband emission, which is typical for LII signal, is measured with a low S/N ratio. This suggests that at this fluence, the incandescence signal starts to contribute to the whole spectrum in addition to the fluorescent emissions detected at prompt timing (Fig. 7b). At 20 ns, one might assume that there are still components from non-LII contributions. The spectrometer should therefore detect a mixture of non-LII and LII components of signals. In reality, only the LII broadband emission can be recognized when looking at the spectrum in Fig. 10. Two reasons have been identified to explain this: 1) the LII-like nature of signals are more predominant than non-LII contributions for the considered conditions, and/or 2) the spectrometer used in this study is not accurate enough to successfully separate non-LII and LII components in those spectra.

To summarize, below 0.06 J/cm^2, the dominant laser-induced emission (LIE) of TiO_2 is LIF as shown in Fig. 8 (similar literature can be found in [78] and [79] as well). At 0.1 J/cm^2 and above, two different types of signals can be observed: one from LIF centered at 470 nm over the UV wavelengths, and another at longer wavelength that corresponds to the onset of LII. The threshold for the appearance of LII is more than half of the evaporation fluence of 0.19 J/cm^2. This behavior is not surprising for LII, as its intensity is strongly non-linear with fluence. The gap between the appearance fluence and the evaporation fluence can vary, depending on the excitation wavelength and the nature of the particles. This feature is well known for soot, as illustrated in the case reported by Goulay et al. [80]. For soot particles, a factor of around 4 is observed between the appearance fluence and the evaporation fluence in the case of 1064 nm, and a factor of around 2 is found in the case of 532 nm [80].

For the highest laser fluence (F = 0.24 J/cm^2), the spectrum exhibits incandescence trends as a function of the acquisition delay: the spectrum shifts toward longer wavelengths with time delay. This indicates that temperature decreases during the signal decay due to the cooling of the particles, confirming the black body-like tendency for pure TiO_2. As already discussed for F = 0.1 J/cm^2 at 20 ns and 40 ns, a certain contribution from the emission of LIF or PS-LIBS might exist. Nevertheless, the overall delayed spectra consistently exhibit a red shift as the particle cools. A very similar trend is observed for F = 0.19 J/cm^2 (not shown).

4.1.3 Discussion

The nature of LIE depends strongly on the light–particle interaction, providing indications on the state of the particles. In low fluence regime, laser light can excite the electronic state of particles, leading to the fluorescence without any modification of the particle state, i.e., solid particles are

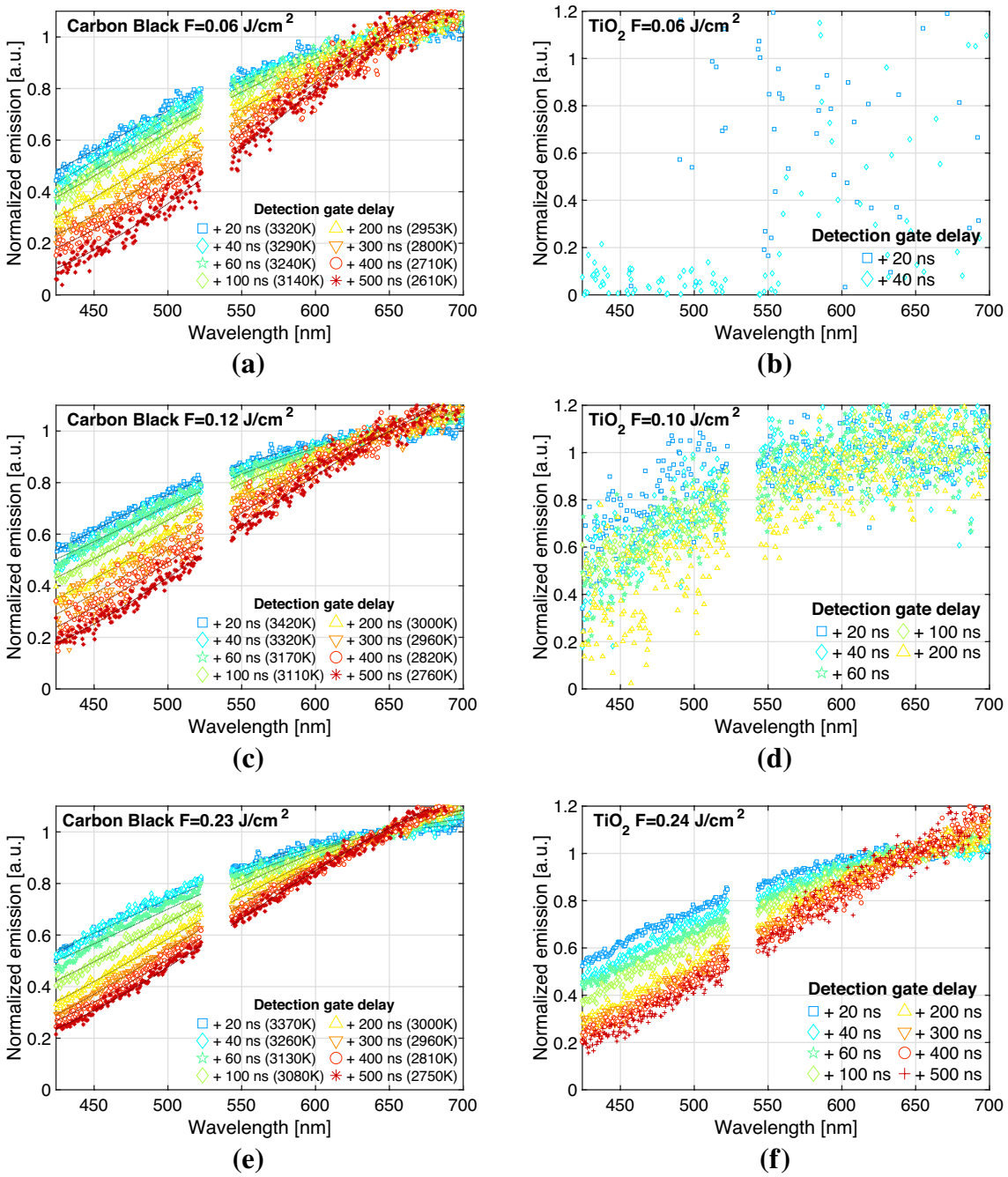

Fig. 10 Effect of gate delay (gate width = 20 ns) on emission spectra of laser-induced emissions of **a**, **c**, **e** carbon black nanoparticles and **b**, **d**, **f** rutile TiO_2 nanoparticles. The temperature given inside the legend for carbon black particles is obtained from spectrum fitting. Spectra are normalized with the value of the spectrum at 650 nm

expected. By increasing the fluence, particles can be thermally heated resulting in the emission of incandescence signals. If the temperature of the particles is higher than the melting point but lower than the boiling point, particles may exist in a liquid state. As discussed in Fig. 2, a higher or lower $E(m_\lambda)$ value can be observed when particles are in a liquid state. If the $E(m_\lambda)$ value is higher in the liquid state than in the solid state, LII measurements can be more easily performed in the intermediate fluences if particles reach the melting temperature. At even higher fluence regime, particles may reach the vaporization temperature so that PS-LIBS emission can be facilitated and observed. By looking at the results in Fig. 7b, it is then possible to deduce some indications on the particle state. On one hand, carbon black nanoparticles are characterized by high $E(m_\lambda)$ values when in solid state and very high melting and boiling points

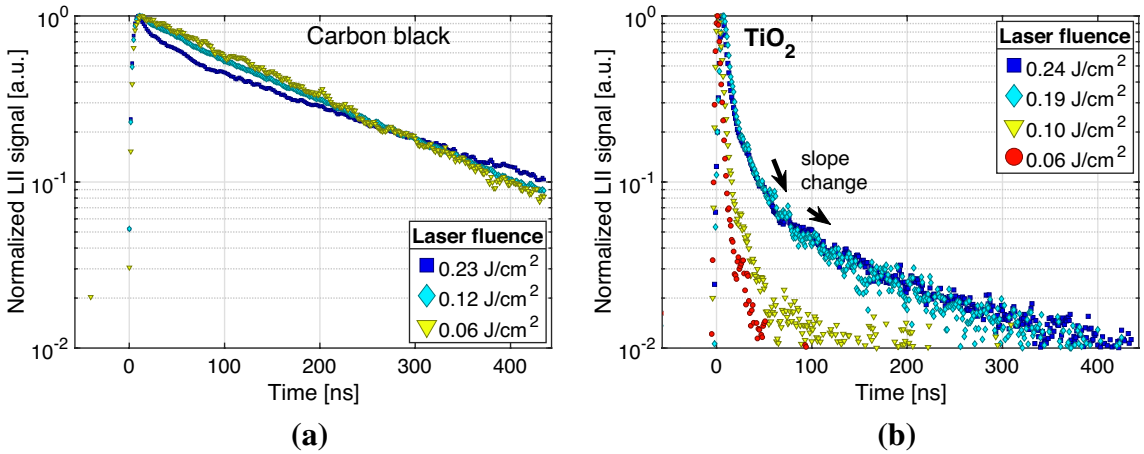

Fig. 11 Temporal evolution of laser-induced emission of **a** carbon black and **b** TiO_2 nanoparticles at 450 ± 10 nm detection wavelength. Each profile is normalized by its maximum value

($T_{\text{meting}}^{\text{carbon black}}$ = 3823 K [81] and $T_{\text{boiling}}^{\text{carbon black}}$ = 4473 K [81], respectively) and it is classically assumed a solid to gas conversion. As a result, LII signal is observed at the lowest fluence considered and a smooth transition is observed until vaporization of carbon atoms is observed for the highest fluence.

On the other hand, TiO_2 nanoparticles have low $E(m_\lambda)$ values when they are in the solid state and lower melting and boiling temperature ($T_{\text{meting}}^{\text{TiO}_2} \sim$ 2100K [58] and $T_{\text{boiling}}^{\text{TiO}_2}$ = 2773–3273 K [82], respectively). It seems then that these particles can hardly be heated, so only LIF is observed at low fluences. For higher fluences, it is possible that particles are initially converted to a liquid state during the heating process. Consequently, $E(m_\lambda)$ increases, which subsequently enhances the particle heating up to their vaporization. As a result, no smooth transition is observed for LIE signals on TiO_2 particles. For small fluences, particles cannot be sufficiently heated due to their low $E(m_\lambda)$. For high fluence regimes, it seems that particles have changed their state, increasing their $E(m_\lambda)$ value and, consequently, enhancing the particle heating process.

In the following section, the temporal behavior is investigated to confirm the conclusions on the nature of LIE.

4.2 Temporal analysis

Before analyzing the temporal evolution of LIE, it is important to remind that the temporal profile is closely related to the primary particle size [30]. In this study, particles of the same size are expected to be distributed into the optical cell during the measurement, whereas a polydisperse population is generally found in flame synthesis. Still, the particle diameter can decrease with time in case of sublimation, i.e., for high laser fluence regimes [83].

The temporal evolution of the signals emitted at 450 nm for carbon black and of TiO_2 under different fluences are presented in Fig. 11. For carbon black (Fig. 11a), the decay rates are relatively linear (in log scale) without significant slope change for all fluences except for F = 0.23 J/cm^2. Since the particle temperatures for F = 0.06 and 0.12 J/cm^2 are quite similar, the decay rates are nearly the same in Fig. 11a. At F = 0.23 J/cm^2, the high fluence induces the sublimation of the particles, resulting in LIF from vaporized species as discussed in Fig. 7a and decreasing the particle diameter. As a consequence, the LII signal has a rapid decay close to the prompt and presents a slope change of around 50 ns.

For pure TiO_2 particles (Fig. 11b), at low laser fluence (F ≤ 0.06 J/cm^2), a short-lifetime signal is detected at 450 nm. Together with previous analysis on the spectrum, this possibly indicates that the LII component, known to be characterized by long decay time, is not observed at this fluence. This is due to the fact the particle temperature is not high enough to emit a detectable LII signal. The lifetime $t_{\text{non-LII}}$ of this signal is estimated to be ≈ 100 ns (FWHM around 10 ns, tail of temporal profile rests until 60 ns). At higher fluences (F ≥ 0.19 J/cm^2), a slope change is observed near $t_{\text{non-LII}}$, indicating the presence of multiple signals with both short and long lifetimes. The short non-LII contributions are predominant over the first $t_{\text{non-LII}}$ and present a significant slope. The long ones dominate the second period of the emission. Comparing F = 0.19 and F = 0.24 J/cm^2 for $t \geq t_{\text{non-LII}}$, the decay rate is nearly identical, meaning that the processes at the origin of the delayed LIE are quite similar for these two fluences. Once again, if the interpretation of temporal emission from soot particles is well established in literature [84], temporal LIE from TiO_2 requires more extensive analysis.

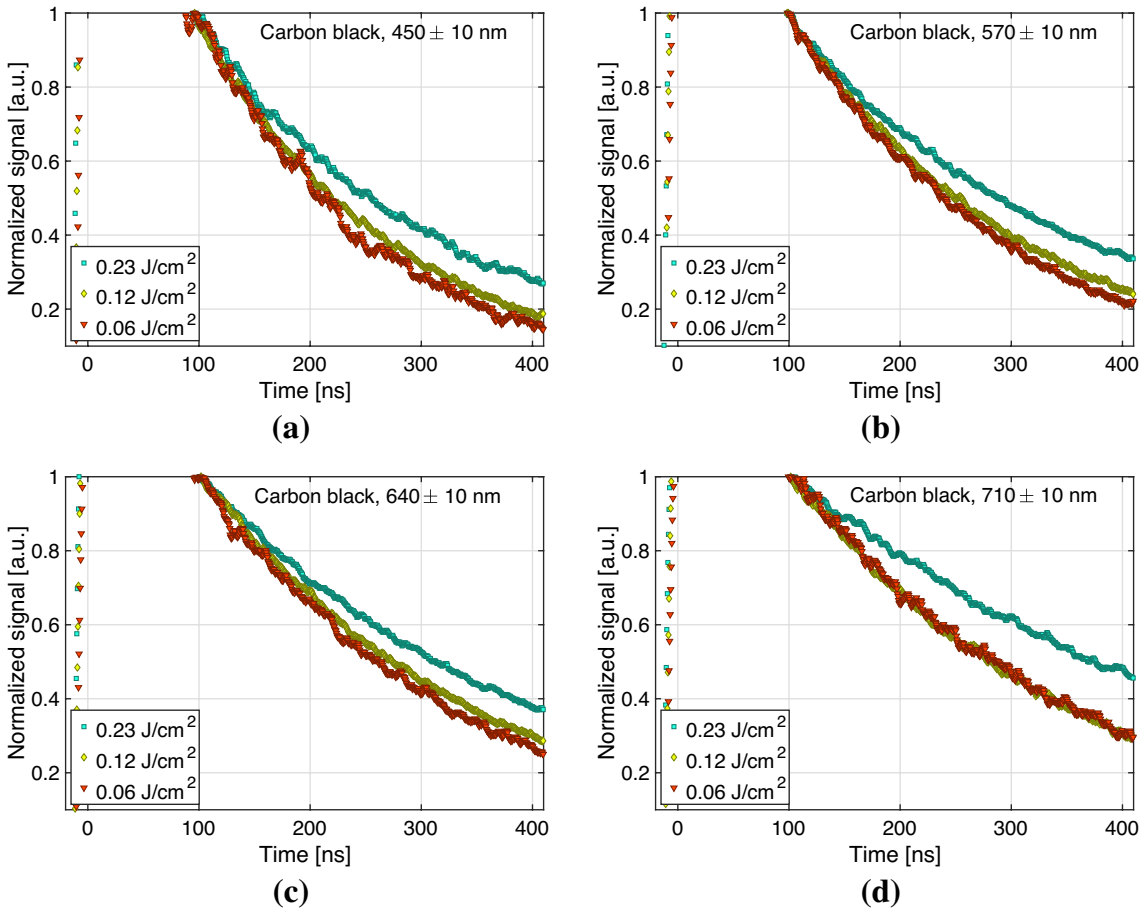

Fig. 12 Normalized temporal evolution of carbon black nanoparticles at different laser fluences at detection wavelengths of **a** 450 ± 10 nm, **b** 570 ± 10 nm, **c** 640 ± 10 nm and **d** 710 ± 10 nm. All profiles are normalized with the value of the signal at 100 ns

For this, Figs. 12 and 13 show the normalized temporal evolution of signal for three different fluences for carbon black and two different fluences for TiO_2 for different detection wavelengths. The temporal evolutions of LIE emissions at four wavelengths are considered for various laser fluences characterized by a significant S/N ratio. Only the temporal signals after 100 ns from peak signal are considered to completely avoid non-LII contribution. The signals are normalized at 100 ns delayed timing to compare the temporal decay.

Concerning carbon black, a shorter residence time is observed when increasing the laser fluence. This is not in contradiction with the LII theory. It is true that at prompt timing for given initial particle state (diameter and temperature), a higher particle temperature is obtained for a higher laser fluence. However, the LII decay rate is governed by the particle temperature gradient as deduced from Eq. 4 and not by particle temperature itself. Such temperature gradient is governed by the evaporation, radiation and conduction processes. Thus, when considering LII in cold environment, it is possible to observe longer decay times for higher laser fluences due to a strong contribution of conduction to the cooling process as proven by LII simulations provided as Supplementary materials.

In the case of TiO_2, the curves exhibit the same decay tendency for all fluences and wavelengths implying that particles have reached relatively close temperatures for the two considering fluences.

To validate the LII nature of the delayed LIE, the decay characteristic time τ is calculated using Eq. (3) by fitting the LIE signals between 100 and 400 ns after the peak signal by using a log function. Results are shown in Figs. 14a and 14b for carbon black and TiO_2, respectively. Here, the fluence values before the evident vaporization regime (at the beginning of the plateau curves) are considered, i.e., $F = 0.12$ J/cm^2 and $F = 0.19$ J/cm^2 for carbon black and high-purity TiO_2, respectively. For other laser fluences, the same linear tendencies have been observed (not shown).

Concerning carbon black nanoparticles, the decay characteristic time τ increases with the wavelength in accordance with Eq. (4), which has been derived for LII signals assuming a constant primary particle diameter d_p. Similarly, for pure TiO_2 nanoparticles, the decay characteristic time τ

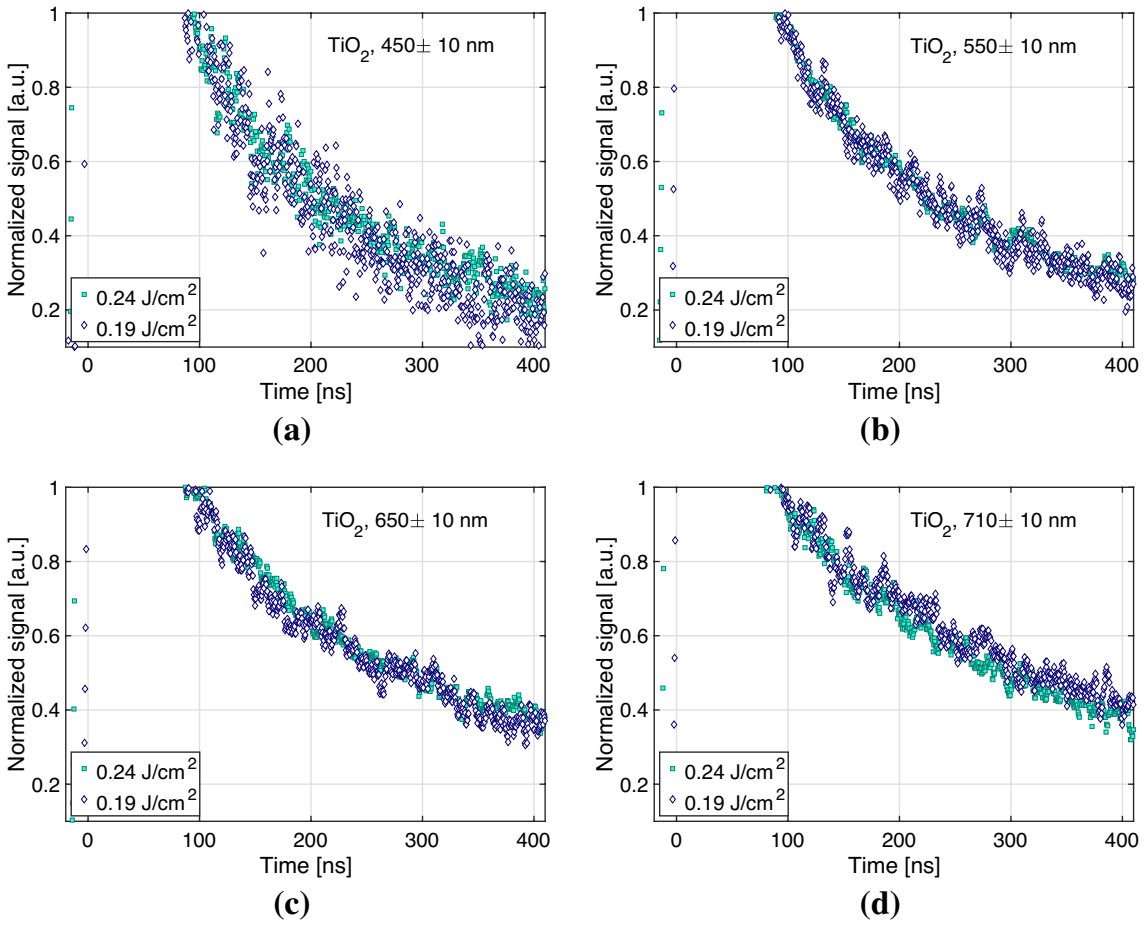

Fig. 13 Normalized temporal evolution of high-purity TiO_2 nanoparticles at different laser fluences at detection wavelengths of **a** 450 ± 10, **b** 550 ± 10, **c** 650 ± 10 and **d** 710 ± 10 nm. All profiles are normalized with the value of the signal at 100 ns

values are linearly proportional to the emission wavelength, confirming the LII nature of the delayed LIE as derived from the LII theory of Sect. 2.1.

Finally, the temporal evolution of quantity ΔT^{-1} defined in Eq. (5) is reported for carbon black nanoparticles in

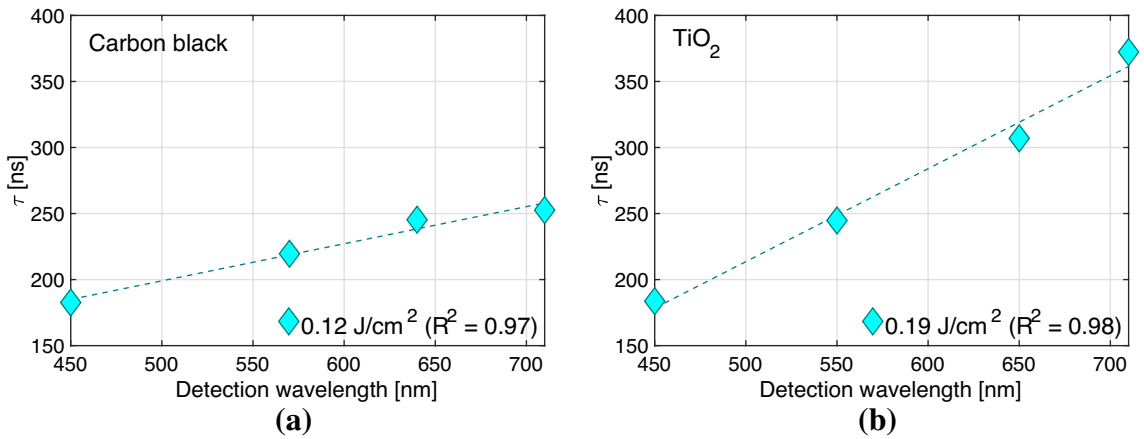

Fig. 14 Decay characteristic times of LIE signal for **a** carbon black and **b** TiO_2 as a function of detection wavelength. The R^2 value inside the legend represents the coefficient of determination for the fitting procedure. The dotted lines are the results of the linear fitting

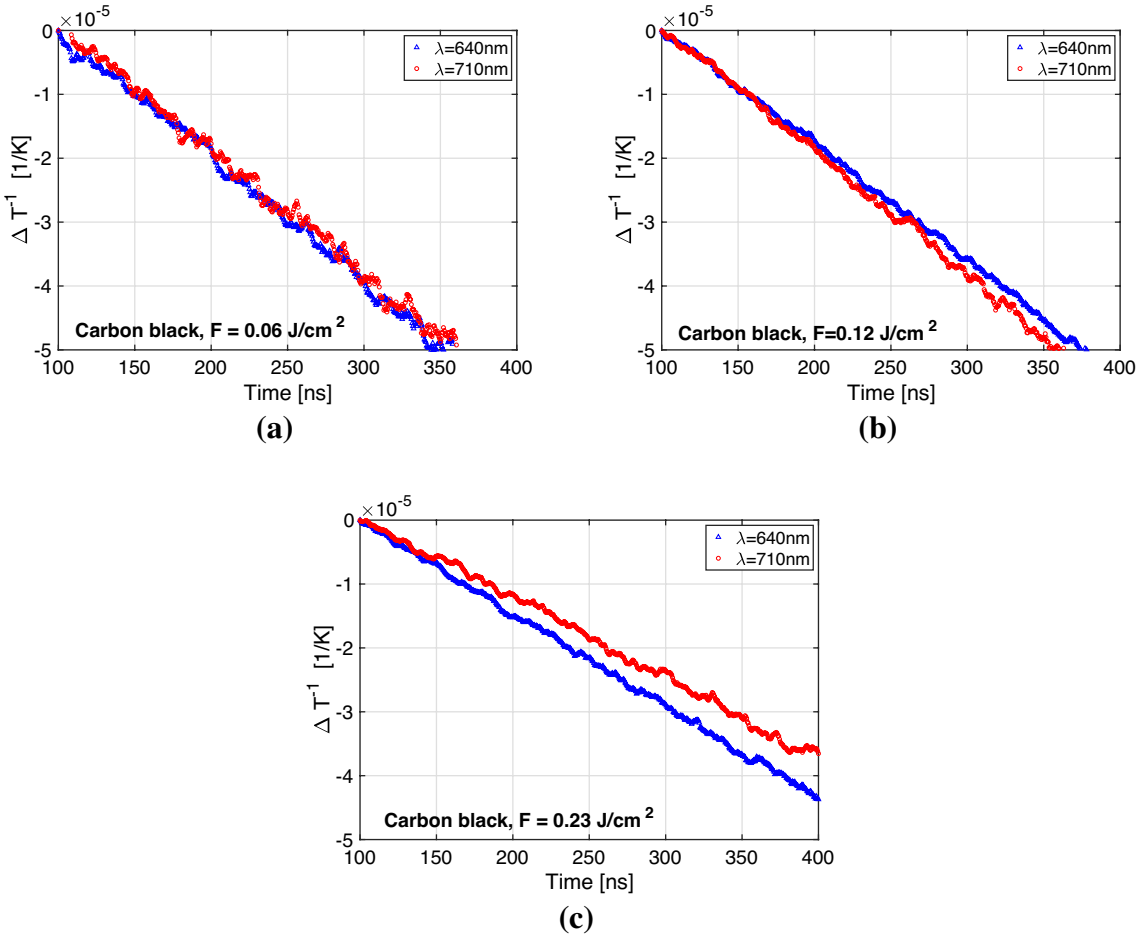

Fig. 15 Time evolution of ΔT^{-1} of carbon black nanoparticles LIE for three laser fluences at **a** $F = 0.06$, **b** $F = 0.12$ and **c** $F = 0.23$ J/cm^2

Fig. 15 for two wavelengths and various fluences from the temporal LIE profile starting at $t_0 = 100$ ns from prompt. In the case of carbon black, the ΔT^{-1} for $\lambda_{em} = 640$ and 710 nm are identical for fluences of 0.06 and 0.12 J/cm^2, confirming the incandescent nature of signal for all signal durations. Once again, discrepancies are observed for the highest fluence ($F = 0.23$ J/cm^2), where sublimation is suspected. The evolution of ΔT^{-1} of TiO_2 of high purity in an inert environment is illustrated in Fig. 16. The evolution of ΔT^{-1} at λ_{em}= 650 nm and λ_{em} =710 nm shows the same decreasing tendency for the two fluence values. Therefore, the LII behavior of pure TiO_2 is demonstrated at least for the LIE signals at these wavelengths and time delays.

5 Conclusion

Laser diagnostics are increasingly employed for the characterization of nanoparticle production in flame synthesis. Among the different available techniques, the LII satisfies the need to characterize the volume fraction with an in situ approach with possible application to turbulent flames. However, the adaptation of LII from conventional soot particles to non-soot metal oxide nanoparticles can be challenging in terms of phase change during the LII process, the selection of excitation laser wavelength, and the existence of non-thermal laser-induced emissions as interference during the measurement. To the authors' knowledge, studies applying LII on TiO_2 have been done until now under the risk of carbon trace in signals from the hydrocarbon fuel or carbon-containing precursors [9, 40, 42, 54]. These studies were mainly performed for high flame temperatures close to the melting point of TiO_2, leading to uncertainty about the source of the incandescent signal. This study aims to definitely assess the feasibility of laser-induced incandescence measurements for TiO_2 nanoparticles by considering high-purity TiO_2 aerosol.

The spectral and temporal behavior of laser-induced emission of TiO_2 were investigated by comparison with carbon black nanoparticles. High-purity TiO_2 produced by sol–gel process and carbon black nanoparticles are dispersed by N_2 gas flow into a non-reacting optical cell. A nearly

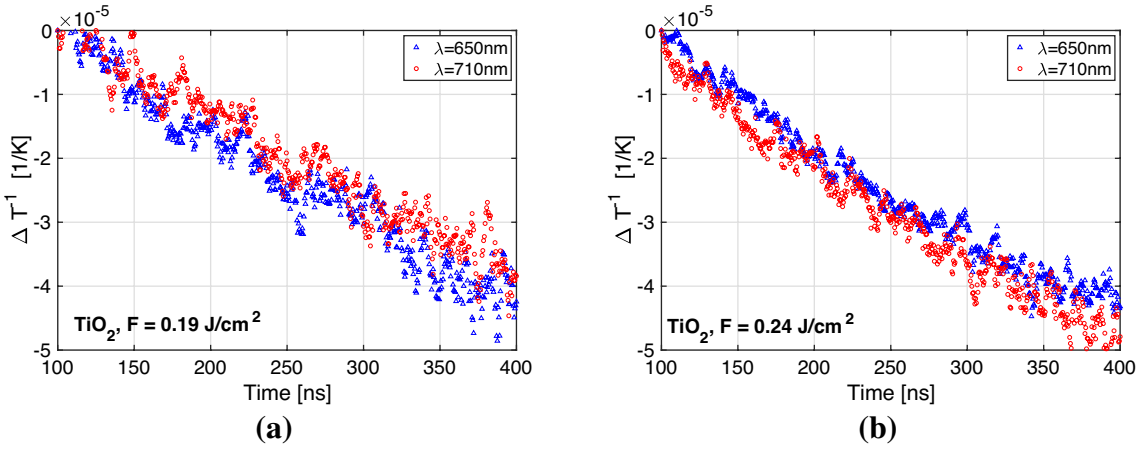

Fig. 16 Time evolution of ΔT^{-1} of pure TiO_2 nanoparticles LIE for two laser fluences at **a** $F = 0.19$ and **b** $F = 0.24$ J/cm^2

top-hat-shaped laser at 355 nm successfully heats the particles. Their spectral and temporal behavior was measured via spectrometer and PMT, respectively. The ambient temperature inert gas dispersion prevents the melting before the laser irradiation, the interference from flame-generated emission, and the possible formation of a carbonaceous layer on the particles.

For carbon black, the blue shift with increasing fluence was observed. C_2 emission was observed at high laser fluence possibly due to sublimation. TiO_2 nanoparticles show different prompt emission spectra depending on the laser fluence. At low fluence, the emission spectra of TiO_2 resemble those reported in the literature for LIF with a minor dissimilarity due to the difference in particle nature and/or experimental parameters. At high fluence, sharp emission features superimposed with broadband emission spectra were detected. The distinct features might be interpreted as narrower LIF emissions under higher fluence or PS-LIBS atomic line emission. Focusing on the part of the signal not influenced by the interferences, the experimental system is validated with conventional carbon black particles by demonstrating that the emission spectra with a delayed gate follow the black-body radiation behavior. Then, for titania, despite the difficulties in excitation and detection of LII measurements due to a small absorption function $E(m_\lambda)$, the delayed gate emission spectra show that the TiO_2 nanoparticles present a black-body-like radiation response during the cooling process. The LII on pure TiO_2 is possible when (1) particles are heated with enough laser fluence and (2) delayed detection is applied to avoid short-duration non-LII emissions. In a temporally resolved signal, those interferences disappear after 100 ns with an apparent change of the decaying slope. The LII nature of TiO_2 LIE is also proven based on the LII theory with temporal evolution in different emission wavelengths.

This study demonstrates the possibility of the in situ LII on pure TiO_2 in a cold environment. In the Supplementary materials, its feasibility is extended to flame-synthesized TiO_2 nanoparticles. Nevertheless, the analysis of the LII signal for non-soot nanoparticles remains challenging. Specifically, the parasite laser-induced emissions, LIF and PS-LIBS atomic emissions, prevent the possibility of measuring the effective temperature of particles at the timing of the signal peak, which is necessary to interpret the LII signal in terms of volume fraction. Data analysis to obtain size information will be more difficult with unknown and/or unfavorable optical properties. The possible coexistence of different particle populations should also be taken into account during the LII signal interpretation.

Supplementary Information The online version contains supplementary material available at https://doi.org/10.1007/s00340-023-08038-3.

Acknowledgements This project has received the European Research Council (ERC) support under the European Union's Horizon 2020 research and innovation program (Grant agreement no. 757912). The authors thank Dr. G. E. (Jay) Jellison of the Oak Ridge National Lab and Dr. Han-Yin Liu at National Sun Yat-Sen University for providing data for the refractive index and extinction coefficient.

Author Contributions JY built the experimental setup, performed the experiments, post-processed the experimental data, and prepared the figure. JY and CB designed the experimental setup. CB and BF defined the scientific strategy. C B, BF, and ND supervised the research. BF found the funding. JY wrote the first version of the manuscript. CB and BF extensively revised the manuscript. All authors reviewed the manuscript.

Declarations

Conflict of interest All authors declare that they have no conflicts of interest.

References

1. F. Meierhofer, U. Fritsching, Synthesis of metal oxide nanoparticles in flame sprays: review on process technology, modeling, and diagnostics. Energy & Fuels **35**(7), 5495–5537 (2021)
2. H.G. Völz, J. Kischkewitz, P. Woditsch, A. Westerhaus, W.-D. Griebler, M. De Liedekerke, G. Buxbaum, H. Printzen, M. Mansmann, D. Räde et al., Pigments, inorganic. Ullmann's Encyclopedia of Industrial Chemistry (2000)
3. S. Zahmatkesh, M. Hajiaghaei-Keshteli, A. Bokhari, S. Sundaramurthy, B. Panneerselvam, Y. Rezakhani, Wastewater treatment with nanomaterials for the future: A state-of-the-art review. Environmental Research, 114652 (2022)
4. X. Hou, K. Aitola, P.D. Lund, TiO_2 nanotubes for dye-sensitized solar cells-a review. Energy Science & Engineering **9**(7), 921–937 (2021)
5. P. Roth, Particle synthesis in flames. Proceedings of the combustion institute **31**(2), 1773–1788 (2007)
6. S.E. Pratsinis, Flame aerosol synthesis of ceramic powders. Progress in Energy and Combustion Science **24**(3), 197–220 (1998)
7. M.Y. Manuputty, C.S. Lindberg, J.A. Dreyer, J. Akroyd, J. Edwards, M. Kraft, Understanding the anatase-rutile stability in flame-made TiO_2. Combustion and Flame **226**, 347–361 (2021)
8. Y. Ren, K. Ran, S. Kruse, J. Mayer, H. Pitsch, Flame synthesis of carbon metal-oxide nanocomposites in a counterflow burner. Proceedings of the Combustion Institute **38**(1), 1269–1277 (2021)
9. F. Cignoli, C. Bellomunno, S. Maffi, G. Zizak, Laser-induced incandescence of titania nanoparticles synthesized in a flame. Applied Physics B **96**(4), 593–599 (2009)
10. N.K. Memon, D.H. Anjum, S.H. Chung, Multiple-diffusion flame synthesis of pure anatase and carbon-coated titanium dioxide nanoparticles. Combustion and flame **160**(9), 1848–1856 (2013)
11. C. Russo, B. Apicella, A. Tregrossi, A. Ciajolo, K.C. Le, S. Török, P.-E. Bengtsson, Optical band gap analysis of soot and organic carbon in premixed ethylene flames: Comparison of in-situ and ex-situ absorption measurements. Carbon **158**, 89–96 (2020)
12. T.A. Sipkens, J. Menser, T. Dreier, C. Schulz, G.J. Smallwood, K.J. Daun, Laser-induced incandescence for non-soot nanoparticles: recent trends and current challenges. Applied Physics B **128**(4), 1–31 (2022)
13. H.A. Michelsen, Laser-induced incandescence of flame-generated soot on a picosecond time scale. Applied Physics B **83**(3), 443–448 (2006)
14. J. Liqiang, Q. Yichun, W. Baiqi, L. Shudan, J. Baojiang, Y. Libin, F. Wei, F. Honggang, S. Jiazhong, Review of photoluminescence performance of nano-sized semiconductor materials and its relationships with photocatalytic activity. Solar Energy Materials and Solar Cells **90**(12), 1773–1787 (2006)
15. N. Serpone, D. Lawless, R. Khairutdinov, Size effects on the photophysical properties of colloidal anatase TiO_2 particles: size quantization versus direct transitions in this indirect semiconductor? The journal of Physical Chemistry **99**(45), 16646–16654 (1995)
16. C.C. Mercado, F.J. Knorr, J.L. McHale, S.M. Usmani, A.S. Ichimura, L.V. Saraf, Location of hole and electron traps on nanocrystalline anatase TiO_2. The Journal of Physical Chemistry C **116**(19), 10796–10804 (2012)
17. K. Fujihara, S. Izumi, T. Ohno, M. Matsumura, Time-resolved photoluminescence of particulate TiO_2 photocatalysts suspended in aqueous solutions. Journal of Photochemistry and Photobiology A: Chemistry **132**(1–2), 99–104 (2000)
18. J. Shi, J. Chen, Z. Feng, T. Chen, Y. Lian, X. Wang, C. Li, Photoluminescence characteristics of TiO_2 and their relationship to the photoassisted reaction of water/methanol mixture. The journal of physical chemistry C **111**(2), 693–699 (2007)
19. D.K. Pallotti, L. Passoni, P. Maddalena, F. Di Fonzo, S. Lettieri, Photoluminescence mechanisms in anatase and rutile TiO_2. The Journal of Physical Chemistry C **121**(16), 9011–9021 (2017)
20. J. Zhang, X. Chen, Y. Shen, Y. Li, Z. Hu, J. Chu, Synthesis, surface morphology, and photoluminescence properties of anatase iron-doped titanium dioxide nano-crystalline films. Physical Chemistry Chemical Physics **13**(28), 13096–13105 (2011)
21. P.B. Nair, V. Justinvictor, G.P. Daniel, K. Joy, K.J. Raju, D.D. Kumar, P. Thomas, Optical parameters induced by phase transformation in rf magnetron sputtered TiO_2 nanostructured thin films. Progress in Natural Science: Materials International **24**(3), 218–225 (2014)
22. Y. Zhang, S. Li, Y. Ren, Q. Yao, C.K. Law, Two-dimensional imaging of gas-to-particle transition in flames by laser-induced nanoplasmas. Applied Physics Letters **104**(2), 023115 (2014)
23. Y. Zhang, S. Li, Y. Ren, Q. Yao, D.T. Stephen, A new diagnostic for volume fraction measurement of metal-oxide nanoparticles in flames using phase-selective laser-induced breakdown spectroscopy. Proceedings of the Combustion Institute **35**(3), 3681–3688 (2015)
24. Y. Ren, J. Wei, S. Li, In-situ laser diagnostic of nanoparticle formation and transport behavior in flame aerosol deposition. Proceedings of the Combustion Institute **37**(1), 935–942 (2019)
25. Y. Ren, Y. Zhang, S. Li, C.K. Law, Doping mechanism of vanadia/titania nanoparticles in flame synthesis by a novel optical spectroscopy technique. Proceedings of the Combustion Institute **35**(2), 2283–2289 (2015)
26. Y. Ren, Y. Zhang, S. Li, Simultaneous single-shot two-dimensional imaging of nanoparticles and radicals in turbulent reactive flows. Physical Review Applied **13**(4), 044002 (2020)
27. Y. Zhang, G. Xiong, S. Li, Z. Dong, S.G. Buckley, D.T. Stephen, Novel low-intensity phase-selective laser-induced breakdown spectroscopy of TiO_2 nanoparticle aerosols during flame synthesis. Combustion and flame **160**(3), 725–733 (2013)
28. G. Xiong, S. Li, D.T. Stephen, Tuning excitation laser wavelength for secondary resonance in low-intensity phase-selective laser-induced breakdown spectroscopy for in-situ analytical measurement of nanoaerosols. Spectrochimica Acta Part B: Atomic Spectroscopy **140**, 13–21 (2018)
29. A.C. Eckbreth, Effects of laser-modulated particulate incandescence on raman scattering diagnostics. Journal of Applied Physics **48**(11), 4473–4479 (1977)
30. S. Will, S. Schraml, A. Leipertz, Two-dimensional soot-particle sizing by time-resolved laser-induced incandescence. Optics letters **20**(22), 2342–2344 (1995)
31. L.A. Melton, Soot diagnostics based on laser heating. Applied optics **23**(13), 2201–2208 (1984)
32. B.F. Kock, C. Kayan, J. Knipping, H.R. Orthner, P. Roth, Comparison of lii and tem sizing during synthesis of iron particle chains. Proceedings of the Combustion Institute **30**(1), 1689–1697 (2005)
33. K. Daun, J. Menser, R. Mansmann, S.T. Moghaddam, T. Dreier, C. Schulz, Spectroscopic models for laser-heated silicon and copper nanoparticles. Journal of Quantitative Spectroscopy and Radiative Transfer **197**, 3–11 (2017)
34. R.L. Vander Wal, T.M. Ticich, J.R. West, Laser-induced incandescence applied to metal nanostructures. Applied optics **38**(27), 5867–5879 (1999)
35. I. Altman, D. Lee, J. Chung, J. Song, M. Choi, Light absorption of silica nanoparticles. Physical Review B **63**(16), 161402 (2001)
36. R. Weeks, W. Duley, Aerosol-particle sizes from light emission during excitation by tea CO_2 laser pulses. Journal of Applied physics **45**(10), 4661–4662 (1974)

37. B. Tribalet, A. Faccinetto, T. Dreier, C. Schultz, Evaluation of particle sizes of iron-oxide nano-particles in a low-pressure flame-synthesis reactor by simultaneous application of tire-lii and pms, in 5th Workshop on Laser-induced Incandescence (2012)
38. A. Eremin, E. Gurentsov, E.Y. Mikheyeva, S. Musikhin, Binary iron–carbon nanoparticle synthesis in photolysis of $Fe(CO)_5$ with methane and acetylene, in Journal of Physics: Conference Series, vol. 774, p. 012127 (2016). IOP Publishing
39. A. Eremin, E. Gurentsov, S. Musikhin, Synthesis of binary iron-carbon nanoparticles by UV laser photolysis of $Fe(CO)_5$ with various hydrocarbons. Materials Research Express **3**(10), 105041 (2016)
40. S. Maffi, F. Cignoli, C. Bellomunno, S. De Iuliis, G. Zizak, Spectral effects in laser induced incandescence application to flame-made titania nanoparticles. Spectrochimica Acta Part B: Atomic Spectroscopy **63**(2), 202–209 (2008)
41. G. De Falco, M. Commodo, P. Minutolo, A. D'Anna, Flame aerosol synthesis and thermophoretic deposition of superhydrophilic TiO_2 nanoparticle coatings. Chemical Engineering Transactions **73**, 37–42 (2019)
42. S. De Iuliis, R. Dondè, I. Altman, Light emission of flame-generated TiO_2 nanoparticles: Effect of ir laser irradiation. Journal of Quantitative Spectroscopy and Radiative Transfer **258**, 107353 (2021)
43. H.K. Kammler, S.E. Pratsinis, Carbon-coated titania nanostructured particles: Continuous, one-step flame-synthesis. Journal of materials research **18**(11), 2670–2676 (2003)
44. M. Darmenkulova, M. Aitzhanov, S.A. Zhumatova, M. Ibraimov, Y. Sagidolda, Change of optical properties of carbon-doped silicon nanostructures under the influence of a pulsed electron beam. Journal of Nanotechnology **2022** (2022)
45. F. Liu, J. Yon, A. Fuentes, P. Lobo, G.J. Smallwood, J.C. Corbin, Review of recent literature on the light absorption properties of black carbon: Refractive index, mass absorption cross section, and absorption function. Aerosol Science and Technology **54**(1), 33–51 (2020)
46. T.C. Williams, C.R. Shaddix, K.A. Jensen, J.M. Suo-Anttila, Measurement of the dimensionless extinction coefficient of soot within laminar diffusion flames. International Journal of Heat and Mass Transfer **50**(7–8), 1616–1630 (2007)
47. Ü.Ö. Köylü, G.M. Faeth, Spectral Extinction Coefficients of Soot Aggregates From Turbulent Diffusion Flames. Journal of Heat Transfer **118**(2), 415–421 (1996)
48. H.-C. Chang, T. Charalampopoulos, Determination of the wavelength dependence of refractive indices of flame soot. Proceedings of the Royal Society of London. Series A: Mathematical and Physical Sciences **430**(1880), 577–591 (1990)
49. D.R. Snelling, F. Liu, G.J. Smallwood, Ö.L. Gülder, Determination of the soot absorption function and thermal accommodation coefficient using low-fluence lii in a laminar coflow ethylene diffusion flame. Combustion and flame **136**(1–2), 180–190 (2004)
50. S. Sarkar, V. Gupta, M. Kumar, J. Schubert, P.T. Probst, J. Joseph, T.A. König, Hybridized guided-mode resonances via colloidal plasmonic self-assembled grating. ACS applied materials & interfaces **11**(14), 13752–13760 (2019)
51. T. Siefke, S. Kroker, K. Pfeiffer, O. Puffky, K. Dietrich, D. Franta, I. Ohlídal, A. Szeghalmi, E.-B. Kley, A. Tünnermann, Materials pushing the application limits of wire grid polarizers further into the deep ultraviolet spectral range. Adv. Opt. Mater. **4**(11), 1780–1786 (2016)
52. H.-Y. Liu, Y.-L. Hsu, H.-Y. Su, R.-C. Huang, F.-Y. Hou, G.-C. Tu, W.-H. Liu, A comparative study of amorphous, anatase, rutile, and mixed phase TiO_2 films by mist chemical vapor deposition and ultraviolet photodetectors applications. IEEE Sens. J. **18**(10), 4022–4029 (2018)
53. G. Jellison Jr., L. Boatner, J. Budai, B.-S. Jeong, D. Norton, Spectroscopic ellipsometry of thin film and bulk anatase (TiO_2). J. Appl. Phys. **93**(12), 9537–9541 (2003)
54. S. De Iuliis, F. Migliorini, R. Dondè, Laser-induced emission of tio 2 nanoparticles in flame spray synthesis. Appl. Phys. B **125**(11), 1–11 (2019)
55. H.A. Michelsen, Understanding and predicting the temporal response of laser-induced incandescence from carbonaceous particles. J. Chem. Phys. **118**(15), 7012–7045 (2003)
56. F. Goulay, P.E. Schrader, L. Nemes, M.A. Dansson, H.A. Michelsen, Photochemical interferences for laser-induced incandescence of flame-generated soot. Proc. Combust. Inst. **32**(1), 963–970 (2009)
57. T. Posch, F. Kerschbaum, D. Fabian, H. Mutschke, J. Dorschner, A. Tamanai, T. Henning, Infrared properties of solid titanium oxides: exploring potential primary dust condensates. Astrophys. J. Suppl. Ser. **149**(2), 437 (2003)
58. M.J. O'Neil, A. Smith, P.E. Heckelman, S. Budavari, *The Merck Index—An Encyclopedia of Chemicals, Drugs, and Biologicals. Whitehouse Station* (Merck and co. Inc, New Jersey, 2001), p.4342
59. J.C. Miller, Optical properties of liquid metals at high temperatures. Philos. Mag. **20**(168), 1115–1132 (1969)
60. D.L. Parry, M.Q. Brewster, Optical constants of Al_2O_3 smoke in propellant flames. J. Thermophys. Heat Transf. **5**(2), 142–149 (1991)
61. F. Goulay, L. Nemes, P.E. Schrader, H.A. Michelsen, Spontaneous emission from C_2 ($d^3\Pi_g$) and C_3 ($A\,^1\Pi_u$) during laser irradiation of soot particles. Mol. Phys. **108**(7–9), 1013–1025 (2010)
62. Z. Gao, L. Han, J. Li, Investigation of laser induced air breakdown thresholds at 1064, 532, 355, 266 and 248nm, in Pacific Rim Laser Damage 2019: Optical Materials for High-Power Lasers, vol. 11063, pp. 23–27 (2019). SPIE
63. G. Xiong, S. Li, Y. Zhang, S.G. Buckley, D.T. Stephen, Phase-selective laser-induced breakdown spectroscopy of metal-oxide nanoparticle aerosols with secondary resonant excitation during flame synthesis. J. Anal. At. Spectrom. **31**(2), 482–491 (2016)
64. Y. Ren, S. Li, Y. Zhang, D.T. Stephen, M.B. Long, Absorption-ablation-excitation mechanism of laser-cluster interactions in a nanoaerosol system. Phys. Rev. Lett. **114**(9), 093401 (2015)
65. R.F. LeBouf, A.L. Miller, C. Stipe, J. Brown, N. Murphy, A.B. Stefaniak, Comparison of field portable measurements of ultrafine TiO_2: X-ray fluorescence, laser-induced breakdown spectroscopy, and fourier-transform infrared spectroscopy. Environ. Sci. Process. Imp. **15**(6), 1191–1198 (2013)
66. J. Menneveux, F. Wang, S. Lu, X. Bai, V. Motto-Ros, N. Gilon, Y. Chen, J. Yu, Direct determination of ti content in sunscreens with laser-induced breakdown spectroscopy: Line selection method for high TiO_2 nanoparticle concentration. Spectrochim. Acta Part B At. Spectrosc. **109**, 9–15 (2015)
67. R. Noll, *Laser-Induced Breakdown Spectroscopy* (Springer, Heidelberg, 2012)
68. S. Bejaoui, S. Batut, E. Therssen, N. Lamoureux, P. Desgroux, F. Liu, Measurements and modeling of laser-induced incandescence of soot at different heights in a flat premixed flame. Appl. Phys. B **118**(3), 449–469 (2015)
69. Y.J. Lee, N.W. Song, S.K. Kim, Photoluminescence of C_{60} and its photofragments in the gas phase. J. Phys. Chem. A **106**(23), 5582–5590 (2002)
70. E.A. Rohlfing, Optical emission studies of atomic, molecular, and particulate carbon produced from a laser vaporization cluster source. J. Chem. Phys. **89**(10), 6103–6112 (1988)
71. R.L. Vander Wal, G.M. Berger, T.M. Ticich, P.D. Patel, Application of laser-induced incandescence to the detection of carbon nanotubes and carbon nanofibers. Appl. Opt. **41**(27), 5678–5690 (2002)

72. K.K. Paul, P. Giri, Role of surface plasmons and hot electrons on the multi-step photocatalytic decay by defect enriched Ag@ TiO_2 nanorods under visible light. J. Phys. Chem. C **121**(36), 20016–20030 (2017)
73. B. Santara, P. Giri, K. Imakita, M. Fujii, Evidence of oxygen vacancy induced room temperature ferromagnetism in solvothermally synthesized undoped TiO_2 nanoribbons. Nanoscale **5**(12), 5476–5488 (2013)
74. L. Forss, M. Schubnell, Temperature dependence of the luminescence of TiO2 powder. Appl. Phys. B **56**, 363–366 (1993)
75. N.D. Abazović, M.I. Čomor, M.D. Dramićanin, D.J. Jovanović, S.P. Ahrenkiel, J.M. Nedeljković, Photoluminescence of anatase and rutile TiO_2 particles. J. Phys. Chem. B **110**(50), 25366–25370 (2006)
76. Y. Lei, L. Zhang, Fabrication, characterization, and photoluminescence properties of highly ordered TiO_2 nanowire arrays. J. Mater. Res. **16**(4), 1138–1144 (2001)
77. A. Kramida, Yu. Ralchenko, J. Reader, NIST ASD Team NIST Atomic Spectra Database (ver. 5.9), [Online]. Available: https://physics.nist.gov/asd [2022, June 2]. National Institute of Standards and Technology, Gaithersburg, MD (2021)
78. L. De Haart, G. Blasse, The observation of exciton emission from rutile single crystals. J. Solid State Chem. France **61**(1), 135–136 (1986)
79. Y.C. Zhu, C.X. Ding, Investigation on the surface state of TiO_2 ultrafine particles by luminescence. Journal of Solid State Chemistry **145**(2), 711–715 (1999)
80. F. Goulay, P.E. Schrader, X. López-Yglesias, H.A. Michelsen, A data set for validation of models of laser-induced incandescence from soot: temporal profiles of lii signal and particle temperature. Applied Physics B **112**(3), 287–306 (2013)
81. Carbon Black. CAS Common Chemistry. CAS, a Division of the American Chemical Society, (retrieved 2022-05-06) (CAS RN: 1333-86-4). https://commonchemistry.cas.org/detail?cas_rn=1333-86-4
82. R. Weast et al., Crc handbook of chemistry and physics 69th ed (boca raton, fl: Chemical rubber) (1988)
83. H. Michelsen, F. Liu, B.F. Kock, H. Bladh, A. Boïarciuc, M. Charwath, T. Dreier, R. Hadef, M. Hofmann, J. Reimann et al., Modeling laser-induced incandescence of soot: a summary and comparison of lii models. Appl. Phys. B **87**(3), 503–521 (2007)
84. H. Michelsen, C. Schulz, G. Smallwood, S. Will, Laser-induced incandescence: Particulate diagnostics for combustion, atmospheric, and industrial applications. Prog. Energy Combust. Sci. **51**, 2–48 (2015)